Research Article

ADVANCED PHOTONICS

Generating a sub-nanometer-confined optical field in a nanoslit waveguiding mode

Liu Yang,[a,†] Zhanke Zhou,[a,†] Hao Wu,[a] Hongliang Dang,[a] Yuxin Yang,[a] Jiaxin Gao,[a] Xin Guo,[a,b] Pan Wang,[a,b] and Limin Tong[a,b,c,*]

[a]Zhejiang University, College of Optical Science and Engineering, New Cornerstone Science Laboratory, Interdisciplinary Center for Quantum Information, Hangzhou, China
[b]Jiaxing Institute of Zhejiang University, Intelligent Optics and Photonics Research Center, Jiaxing, China
[c]Shanxi University, Collaborative Innovation Center of Extreme Optics, Taiyuan, China

Abstract. We propose to generate a sub-nanometer-confined optical field in a nanoslit waveguiding mode in a coupled nanowire pair (CNP). We show that, when a conventional waveguide mode with a proper polarization is evanescently coupled into a properly designed CNP with a central nanoslit, it can be efficiently channeled into a high-purity nanoslit mode within a waveguiding length <10 μm. The CNP can be either freestanding or on-chip by using a tapered fiber or planar waveguide for input-coupling, with a coupling efficiency up to 95%. Within the slit region, the output diffraction-limited nanoslit mode offers an extremely confined optical field (~0.3 nm × 3.3 nm) with a peak-to-background ratio higher than 25 dB and can be operated within a 200-nm bandwidth. The group velocity dispersion of the nanoslit mode for ultrafast pulsed operation is also briefly investigated. Compared with the previous lasing configuration, the waveguiding scheme demonstrated here is not only simple and straightforward in structural design but is also much flexible and versatile in operation. Therefore, the waveguiding scheme we show here may offer an efficient and flexible platform for exploring light–matter interactions beyond the nanometer scale, and developing optical technologies ranging from superresolution nanoscopy and atom/molecule manipulation to ultra-sensitivity detection.

Keywords: sub-nm; confined optical field; nanoslit; evanescent coupling; waveguide mode.

Received Mar. 7, 2023; revised manuscript received May 9, 2023; accepted for publication Jun. 12, 2023; published online Jul. 7, 2023.

[DOI: 10.1117/1.AP.5.4.046003]

1 Introduction

Generating a light beam or an optical field with tighter spatial confinement is always of great interest in both fundamental research and technological applications ranging from ultratight field confinement,[1–12] nanoscale light–matter interaction,[13–17] to superresolution optical imaging.[18–21] Due to the optical diffraction limit,[22] optical confinement with a conventional dielectric component (e.g., a lens) cannot be better than $\lambda/2n$, where λ is the vacuum wavelength of light and n is the refractive index of the medium. Recently, relying on optical resonance or interference, field confinement down to deep-subwavelength level has been realized in dielectric nanostructures.[1–8,10–13] However, limited by the feature size and the fabrication precision of the functional structure, confining optical field to sub-10 nm (i.e., $\lambda/100$ level for visible or near-infrared light) remains challenging. On the other hand, optical-frequency nanoplasmonics, relying on the collective oscillation of free electrons in nanoscale metallic structures, can now confine an optical field down to 10-nm (i.e., $\lambda/100$ level[23]) or even 1-nm level (i.e., $\lambda/1000$ level[24,25]), and has been explored for various applications, including nanowaveguides, nanolasers, nonlinear optical effects enhancement, and optical sensing.[26–29]

However, at optical frequency, when the plasmon mode is confined down to a certain degree (e.g., $\lambda/100$), the optical loss of oscillating free electrons will increase drastically with the increasing confinement,[30] reducing the coherence of the confined field, regardless of the geometries of the structure.[31] Also, the optical-loss-generated heat in the material will bring thermal

*Address all correspondence to Limin Tong, phytong@zju.edu.cn
†These authors contributed equally to this work.

noise and damage and limit the available optical intensity either. Moreover, from the uncertainty relation ($\Delta x \cdot \Delta p \geq \alpha\hbar$; where $\hbar$ is the reduced Planck constant, α is a constant determined by the field characteristics[32,33]) between the photon position (x) and its momentum (p), to confine a light field to an extremely small spatial size (e.g., reduce Δx to 1-nm level), a huge momentum uncertainty (Δp) is required for compensation, which will significantly increase the momentum mismatch between the free-space propagating wave and the confined optical field.

To circumvent the above-mentioned issues, recently, relying on a nanoslit assembled with bottom-up grown single-crystal nanowires with atomic surface roughness, we realized a sub-nanometer-confined (sub-nm-confined) field in coupled nanowire pair (CNP) lasers.[34] In such a scheme, the probability of photon occurrence (i.e., the field intensity) within the 1-nm-slit was significantly increased by the oscillation of bound electrons in the CdSe nanowire interfaces around the slit, resulting in a sub-nm-confined optical field with high peak-to-background intensity ratio. Meanwhile, since the whole mode area remains large, the momentum of the confined photon, averaged by its occurrence in the background field, is not necessarily to be much larger than the photon momentum in free space. Such a confinement scheme can generate a coherent field with unprecedented sub-nm optical confinement and avoid a large photon momentum mismatch between the confined field and the free-space light. However, as it uses a lasing configuration, the selectivity and tunability of the confined field in time and frequency domains, which are highly desired for practical applications, are limited due to the critical and complicated lasing and pumping conditions in a nanolaser.

Here, we propose a waveguiding scheme to generate a sub-nm-confined optical field in a nanoslit mode. Unlike the lasing approach that actively generates coherent fields via lasing oscillation inside the CNP, here the coherent field comes from light sources outside the CNP and is evanescently coupled into the CNP with high efficiency, making it possible to generate extremely confined optical fields with great flexibilities, such as narrow linewidth, broadband tunability, and ultrafast pulsed operation. We show that, with matched effective refractive indices (n_{eff}), a waveguiding mode from a fiber taper can be evanescently coupled into a CNP with an efficiency of up to 95%, and channeled into the desired nanoslit mode with a purity up to 99%. The confined field also has a sub-nm confinement and a high peak-to-background ratio within a spectral range over 100 nm. In addition, we show that, such a waveguiding scheme also works in the mid-infrared (MIR) spectral range, while maintaining an optical confinement of ~0.2 nm, corresponding to ~1/20,000 vacuum wavelength.

2 Configuration of the CNP Waveguiding Scheme

The CNP waveguiding scheme we proposed here is schematically illustrated in Fig. 1. Light from an outer light source is first coupled into a standard glass fiber and adiabatically guided through a fiber taper fabricated at the other end of the fiber. Then, relying on an evanescent coupling process, it is coupled into a freestanding CNP waveguide from one end, propagating along the properly designed CNP waveguide, in which the waveguided field is evoluted into the nanoslit mode, and finally outputs at the opposite end of the CNP [Fig. 1(a)]. Benefiting from the tapering profile of the fiber taper, the matching of n_{eff}

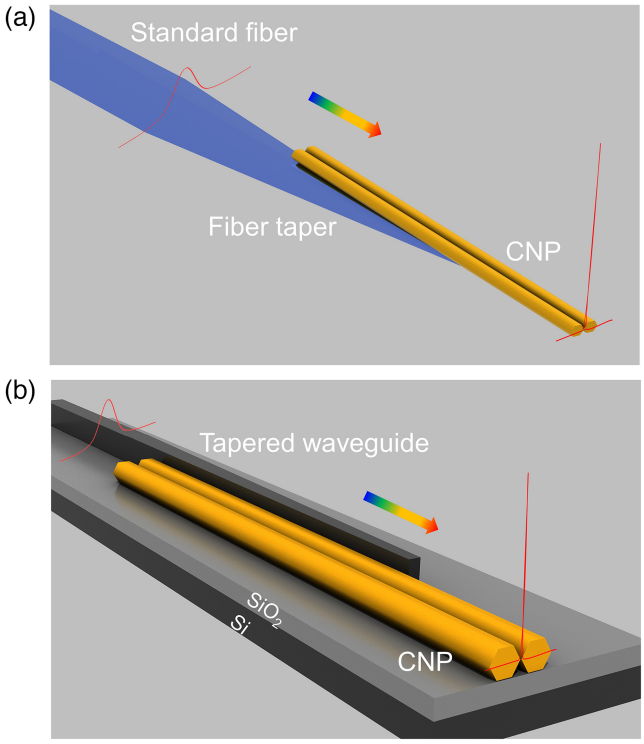

Fig. 1 Schematic illustration of the CNP waveguiding scheme. (a) Freestanding CNP waveguide, coupled by a fiber taper drawn from a standard glass fiber. (b) On-chip CNP waveguide, coupled by a tapered planar waveguide.

between the fiber taper and the CNP can be achieved within a broadband spectral range,[35,36] ensuring a high efficiency when coupling light from the fiber taper to the CNP. Similarly, in an on-chip configuration [Fig. 1(b)], a tapered planar waveguide can be used for coupling light into one end of a silicon-on-insulator-supported CNP with a high efficiency and high-purity nanoslit mode with extreme optical confinement at its center can be obtained at the other end.

Practically, the CNP waveguide can be assembled by two identical single-crystal nanowires, which are cut from one nanowire with a hexagonal cross section and atomic-level smoothness (see Sec. S1 in the Supplemental Material). Based on the sub-nm sidewall roughness, an ultrafine central slit (~1 nm) can be naturally formed along the central axis of the CNP.[34] Besides, material-rich semiconductor nanowires, such as ZnO, CdS, and CdTe, exhibiting high refractive index (e.g., $n \sim 2.37$ @650 nm for CdS[37]) and negligible absorption loss (e.g., absorption coefficient $\sim 1.1 \times 10^{-12}$ cm^{-1} @650 nm for CdS[37]) below the absorption bandgap, can be used for generating sub-nm-confined field from ultraviolet, visible to MIR or even far-infrared bands. It is worth mentioning that in recent years, individual high-quality semiconductor nanowire has been widely used for low-loss optical waveguiding (typical waveguiding loss ~1 dB mm^{-1}).[38–40]

3 Mode Evolution in the CNP

For a nanowire with a noncircular symmetrical cross section, the lowest-order waveguiding mode contains two nondegenerate modes with different polarizations: a horizontal-polarization-dominated TE_0-like mode and a vertical-polarization-dominated

TM_0-like mode (see Sec. S3 in the Supplemental Material).[41] When two identical nanowires with a proper wavelength-to-diameter ratio are assembled into a CNP, strong mode coupling occurs, resulting in a new set of strong coupling-induced waveguiding modes of the CNP. In general, the lowest four modes can be considered as the symmetric/antisymmetric combinations of the two lowest modes. Since the diameter of nanowires (d, defined as the diagonal of the hexagonal cross section of the nanowire) discussed here is relatively small, we plot only the four lowest eigenmodes with corresponding spatial distributions of polarized bound electrons supported in the CNP [Figs. 2(a)–2(d)]. From the spatial distribution of the charge density [right column in Figs. 2(a)–2(d)], the field confinement and enhancement can be clearly seen. For example, in the TE_0-like mode, around the two central opposite vertices, the polarized charge density (with opposite signs) reaches the maximum, leading to the extreme confinement of optical field within the gap. For comparison, the charge density is not concentrated around the central gap in other modes. Therefore, the existence of modes other than TE_0-like mode may not only split a fraction of total mode power but may also serve as an undesired background field. However, n_{eff} of TE_0- and TM_0-like modes are relatively close [Figs. 2(e)–2(h)], especially in the on-chip case [Figs. 2(g) and 2(h)], which is experimentally difficult to separate by selecting the nanowire diameter, due to the error in diameter measurement[42] and the varying refractive index of the nanowire material under different waveguiding powers and temperatures.[43,44] Fortunately, the polarizations of the TE_0- and TM_0-like modes are almost orthogonal, making it possible to selectively launch the TE_0-like mode by controlling the polarization of the input field. For the higher-order modes (here the TE_1- and TM_1-like modes), the much larger cut-off diameters make it possible to separate from the TE_0-like mode, and thus can be easily eliminated by selecting a proper nanowire diameter. Thus, in the following text, we consider CNP that only supports the lowest two modes (i.e., TE_0- and TM_0-like modes), and selectively launch the TE_0-like mode by selecting the polarization of the input field.

We consider the case of a freestanding CNP that is excited by a waveguiding mode from a silica fiber taper. The CdS CNP is assumed to sit symmetrically on the sidewall of the fiber taper, largely overlapped with the fiber taper in length, with a certain length protruding outward [Fig. 3(a)]. To ensure an adiabatic mode transition in the fiber taper, the tapering angle is assumed to be 3 deg.[36] As shown in Fig. 3(b), the input field is assumed to be a TE-polarized HE_{11} mode at 650-nm wavelength, which is efficient in exciting TE-like modes in the CNP, while almost isolated from the TM-like mode due to the orthogonal polarization. To avoid coupling into higher-order modes [Figs. 2(e) and 2(f)], we select a nanowire diameter of 140 nm, which is below the cut-off diameter of the TE_1/TM_1-like modes, while sufficiently larger than the cut-off diameter of the TE_0-like mode.

When the input mode from a standard fiber (i.e., a TE-polarized HE_{11} mode) enters the tapering area, its n_{eff} is initially

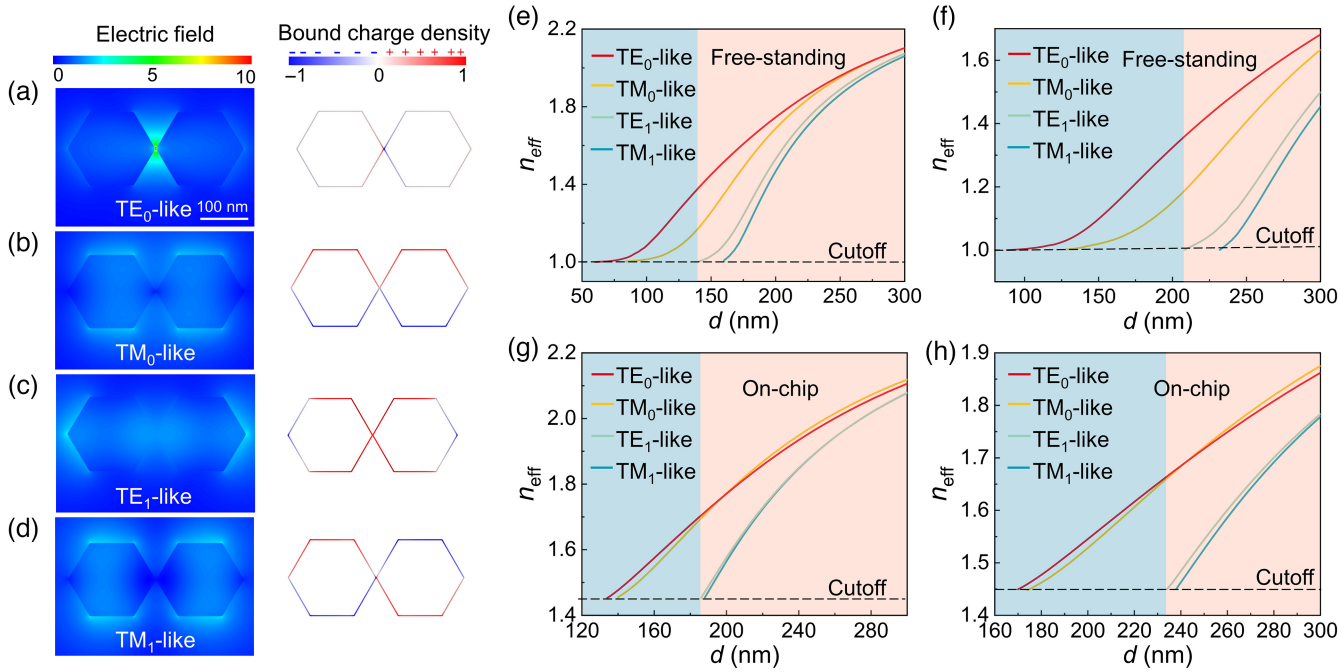

Fig. 2 Four lowest eigenmodes of a CNP waveguide. Normalized electric field distribution (left panel) and surface polarized bound charge density distribution (right panel) of (a) TE_0-like, (b) TM_0-like, (c) TE_1-like, and (d) TM_1-like modes in a CdS CNP with a nanowire diameter of 180 nm at 550-nm wavelength. The scale bar in (a) applies to (b)–(d). (e)–(h) Diameter-dependent n_{eff} of the four lowest modes of (e) a freestanding CNP at 550-nm wavelength, (f) a freestanding CNP at 750-nm wavelength, (g) an on-chip CNP at 550-nm wavelength, and (h) an on-chip CNP at 650-nm wavelength. The blue-shaded areas represent the selected diameter areas in this work. The dashed black lines indicate the refractive index of the substrate.

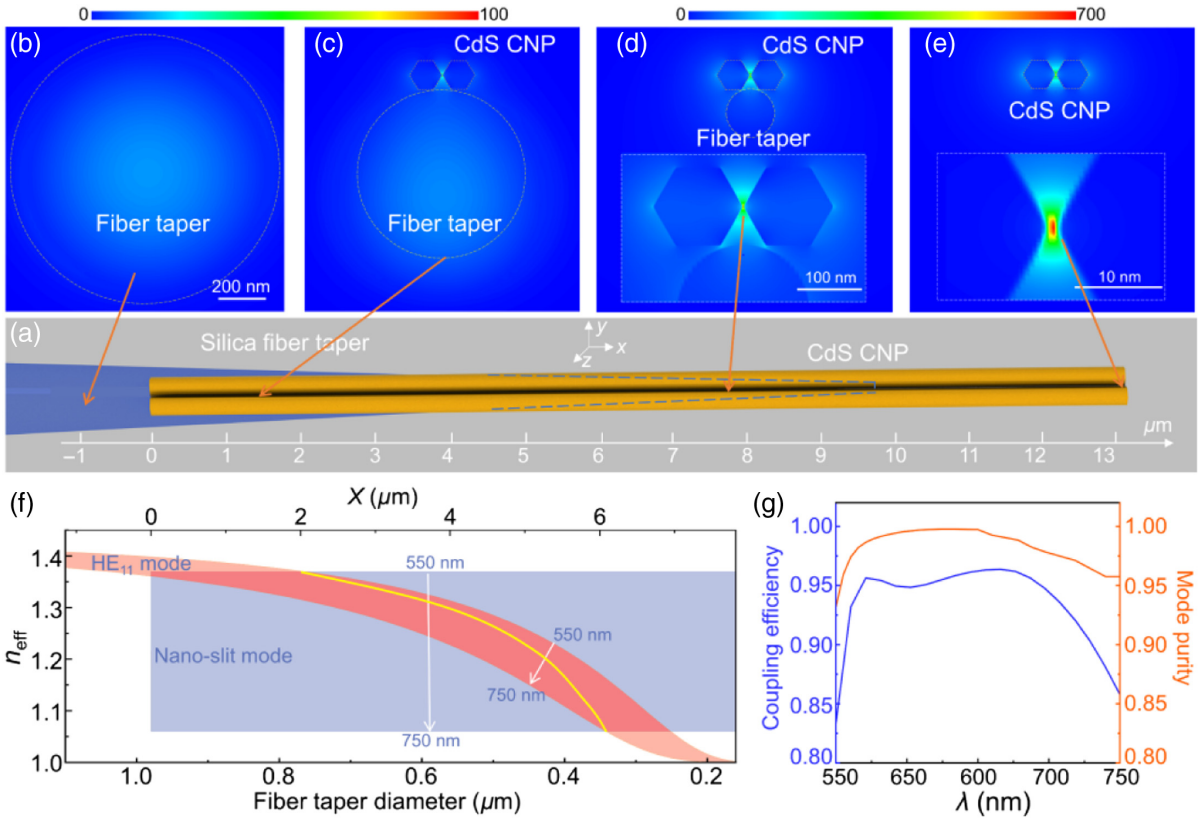

Fig. 3 Mode evolution in a freestanding CdS CNP waveguide. (a) Schematic diagram of the coupling structure. A horizontal coordinate indicates the waveguide length originated from the left end of the CNP. The blue dashed line indicates the obscured profile of the fiber taper beneath the CNP. (b)–(e) Field intensity distribution in $y-z$ planes (cross-sectional planes) at corresponding x positions marked by yellow arrows. The simulation is carried out with a nanowire diameter of 140 nm and a fiber-taper angle of 3 deg at 650-nm wavelength. The insets in (d) and (e) are close-up views of the field intensity around the CNP. The scale bar in (b) applies to (c)–(e). (f) n_{eff} of the HE_{11} mode of the fiber taper and the nanoslit TE_0-like mode of the CNP within the spectral range of 550 to 750 nm. The blue and pink areas indicate the nanoslit mode and the HE_{11} mode, respectively. The intersecting red area is the n_{eff}-matching area of the two modes within the spectral range of 550 to 750 nm, and the solid yellow line represents the matched n_{eff} of the two modes at the same wavelength with respect to the fiber taper diameter (see Sec. S4 in the Supplemental Material). (g) Broadband coupling efficiency and mode purity of the TE_0-like nanoslit mode.

larger than that of the TE_0-like mode of the nanoslit [the leftmost region in Fig. 3(f)]. As it propagates towards the thin end of the fiber taper, the n_{eff} of the input mode decreases with decreasing taper diameter [Fig. 3(f)]. When the n_{eff} of the input mode approaches that of the TE_0-like mode, evident light coupling occurs [Fig. 3(c)]. Benefiting from the properly designed tapering profile of the fiber taper, the coupling length with approximately matched n_{eff} between the two waveguides is optimized for high-efficiency transferring of light from the fiber taper mode into the nanoslit mode [red-colored area in Fig. 3(f)], while almost no light will couple from the nanoslit mode back into the fiber taper mode beyond the n_{eff}-matching area. Eventually, after overlapping area (~9 μm in length), the high-purity nano-slit mode will output from the right-most end of the CNP [Fig. 3(e)].

Owing to a tapering profile and thus a wide-range n_{eff} of the input fiber taper, the waveguiding scheme can be operated within a broad spectral range. For example, when the fiber taper diameter decreases from 1.1 to 0.2 μm, the n_{eff} of the input fiber taper changes from 1.41 to ~1.0 [Fig. 3(f)], which is broad enough for covering the whole range of n_{eff} of the nanoslit mode [Figs. 2(e) and 3(f)], leading to the possibility of efficient excitation of the nanoslit mode within a broad spectral range. Figure 3(g) gives calculated broadband coupling efficiency and mode purity of the excited nanoslit mode output at the right-most end face, showing a broadband high coupling efficiency (>80%) from 550- to 750-nm wavelength, with a maximum efficiency approaching 95% from 569 to 694 nm wavelength.

Within the 200-nm bandwidth (from 550- to 750-nm wavelength), the mode purity of the nanoslit mode (see Sec. S2 in the Supplemental Material) is higher than 93%, with a maximum of 99.8%. The slight impurity may come from the forward-scattering fields (due to the breakage of the symmetry of the

waveguiding structure) and/or a very weak TM_0-like mode (due to the non-strictly orthogonal polarization with TE-polarized mode) that may be excited during the mode coupling and evolution processes.

Also, we have carried out similar calculations for the case of an on-chip CNP, with similar results given in Sec. S5 in the Supplemental Material.

It is worth noting that, when the gap size reduces to 1-nm level, in a metal structure, the nonlocal effect of free electrons (e.g., quantum tunneling,[45] spillover of electrons,[46] and Landau damping[47]) may seriously degrade the field confinement; while in an all-dielectric structure used here, owing to the much stronger localization of the bound electrons, the above-mentioned effects are absent, and the classical electromagnetic field theory is still valid.[48]

4 Sub-nm-Confined Optical Fields in the Waveguiding Nanoslit Mode

To investigate the field distribution of the nanoslit mode in a freestanding CdS CNP, we use a 3-D FDTD simulation for the overall structure and a 2-D COMSOL simulation around the slit area for ultrafine calculation (see Sec. S1 in the Supplemental Material), with results given in Fig. 4. When a 550-nm wavelength light is coupled into and waveguided through a CdS CNP with a nanowire diameter of 140 nm, a slit

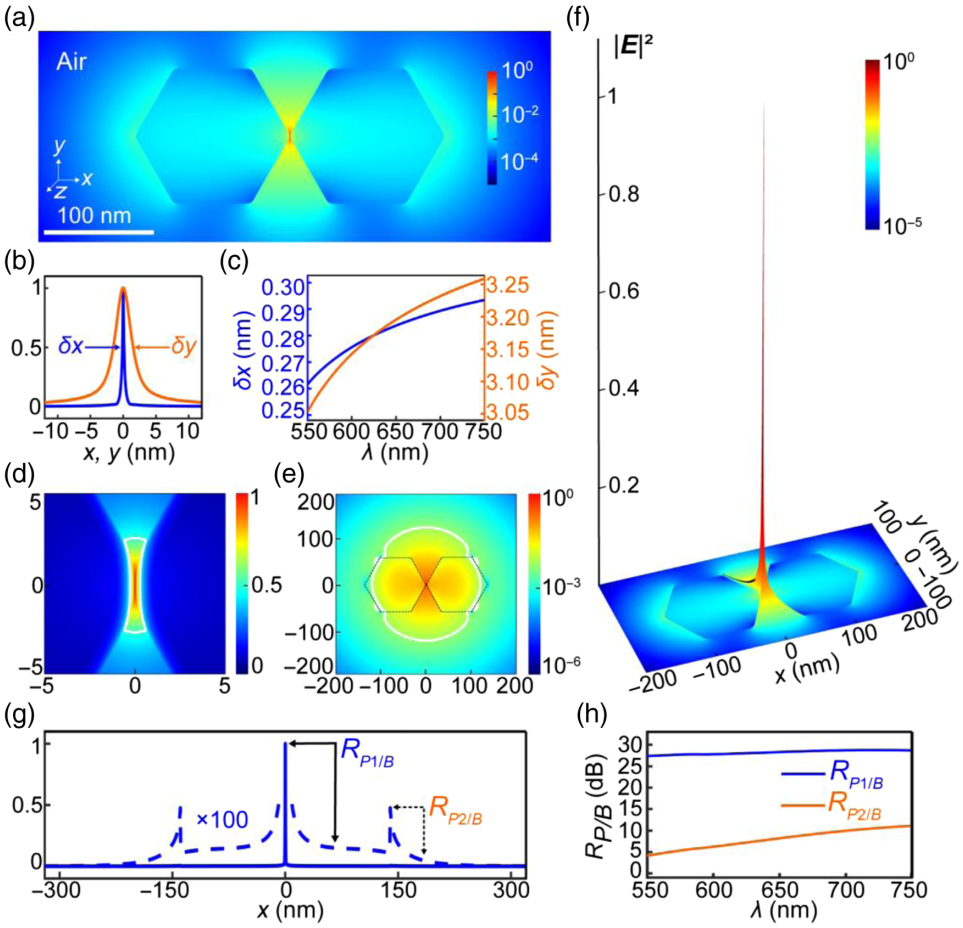

Fig. 4 Sub-nm-confined optical fields in the nanoslit mode at visible spectrum. (a) Normalized cross-sectional field intensity distribution of the TE_0-like nanoslit mode of a CdS CNP with $d = 140$ nm, $w = 1$ nm, $r = 5$ nm, and $\lambda = 550$ nm. The coordinate origin is located at the center of the slit. (b) FWHM of the field intensity of the TE_0-like mode along the x axis (blue line) and y axis (orange line) with $\lambda = 550$ nm. (c) λ-dependent FWHM of the field intensity along the x axis (blue line) and y axis (orange line). (d) Power density (Poynting vector in the z direction, P_z) distribution around the slit cross section. The closed white line indicates the contour of $P_z(0, 0)/2$, marking the profile of the central hot spot. (e) Overall P_z distribution around the CNP cross section in a log scale. The closed white line indicates the boundary of the effective mode area. The units of all coordinates of (d) and (e) are nanometers. (f) 3-D plot of the normalized cross-sectional field intensity distribution of the TE_0-like nanoslit mode. (g) Field intensity distribution along the x-axis direction. For better clarity, a 100× profile is also plotted as dotted lines. (h) λ-dependent peak-to-background ratio $R_{P1/B}$ (blue line) and $R_{P2/B}$ (orange line) of the TE_0-like nanoslit mode, respectively.

width (w) of 1 nm, and a corner radius (r) of 5 nm, the generated TE_0-like slit mode offers a maximum field intensity around the central slit [Fig. 4(a)], with ultratight field confinements of 0.26-nm (x axis) and 3.05-nm (y axis) in full width at half-maximum (FWHM) of the field intensity [Fig. 4(b)]. With increasing wavelength, the FWHM of intensity distribution increases [Fig. 4(c)], mainly due to the decreasing refractive index of the CdS material. Within the broadband from 550 to 750 nm, the field confinement remains a sub-0.3-nm scale (x axis) and a sub-3.3-nm scale (y axis). The calculated spot size is about $1.26 \times 10^{-5}\lambda^2$ ($\sim$4 nm^2) at 550-nm wavelength [Fig. 4(d)], a similar size of a small molecule (e.g., glucose molecule).[49]

Excepting the ultraconfined central field, the overall nanoslit mode is a diffraction-limited optical field [Figs. 4(e) and 4(f)] with an effective mode area[34] of $\sim 0.95(\lambda/n)^2$, which can be considered as a low-intensity large-area background field for averaging the photon momentum of the ultraconfined central field [Fig. 4(f)].

Due to the dielectric noncontinuity of the CNP at the CdS–air interface, besides the central field maximum, there are a series of field maxima in the background field. Figure 4(g) shows the calculated two second-highest peaks (dashed line), which are 23 dB lower in intensity compared with the central peak. By defining a peak-to-background intensity ratio $R_{P1/B}$ between the central peak and the averaged background, and $R_{P2/B}$ between the second-highest peak and the averaged background,[34] we calculate the broadband peak-to-background ratio of the nanoslit mode, with results given in Fig. 4(h). It shows that both ratios increase with increasing wavelength, and $R_{P1/B}$ keeps 27 dB higher than the background and $\sim$20 dB higher than the second-highest peak, which is favorable for using the central peak in applications such as ultraresolution optical nanoscopy and manipulations. In addition, the dependence of the field confinement on the slit width and the corner radius of a CdS CNP waveguide has also been investigated, as shown in Sec. S6 in the Supplemental Material.

It is worth mentioning that, due to its ultralow fraction (e.g., $\sim$0.008% at 550-nm wavelength) of the total mode area, despite its ultrastrong field intensity, the central peak concentrates only a very small fraction (e.g., $\sim$0.19% at 550-nm wavelength) of the total mode power (see Sec. S7 in the Supplemental Material), agreeing well with the low momentum mismatch between the confined field and the free space.

5 Sub-nm-Confined Optical Fields at MIR

Benefiting from the ultrabroadband polarization characteristics (e.g., refractive index, transparency window) of the semiconductor materials such as CdS and CdTe, the operation wavelength of the nanoslit mode in a CNP can be extended to a much broader spectral range. For example, here we investigate field confinement in a CNP operating at the MIR spectrum. We keep the slit width of 1 nm but increase the nanowire diameter to 1 μm according to the much larger wavelength. As shown in Fig. 5, the TE_0-like nanoslit mode can offer an ultratight field confinement in the central slit [Fig. 5(a)], with ultratight field confinements of 0.3-nm (x axis) and 3.2-nm (y axis) in FWHM of the field intensity [Fig. 5(b)], and a spot size of about $3.78 \times 10^{-7}\lambda^2$ at 3.7-μm wavelength [Fig. 5(c)]. The calculated diffraction-limited mode area is about $1.14(\lambda/n)^2$ [Fig. 5(d)]. Interestingly, compared to the visible-spectrum results in Fig. 4(h), here $R_{P1/B}$ is much higher [Fig. 5(e)], owing to the much smaller ratio of the slit size to the wavelength.

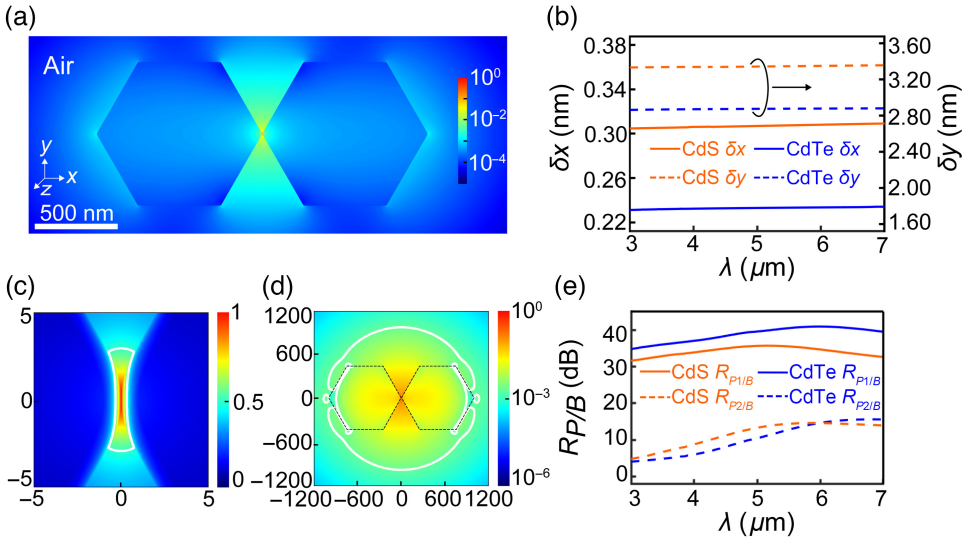

Fig. 5 Sub-nm-confined optical fields in the nanoslit mode at MIR spectrum. (a) Normalized cross-sectional field intensity distribution of the TE_0-like nanoslit mode of a CdS CNP with $d = 1$ μm, $w = 1$ nm, $r = 5$ nm, and $\lambda = 3.7$ μm. (b) λ-dependent FWHM of the field intensity along the x axis (solid line) and y axis (dashed line) of a CdS CNP and a CdTe CNP with the same geometries, respectively. (c) P_z distribution around the slit cross section. The closed white line indicates the contour of $P_z(0, 0)/2$, marking the profile of the central hot spot. (d) Overall P_z distribution around the CNP cross section in a log scale. The closed white line indicates the boundary of the effective mode area. The units of all coordinates of (c) and (d) are nanometers. (e) λ-dependent peak-to-background ratio $R_{P1/B}$ (solid line) and $R_{P2/B}$ (dashed line) of the TE_0-like nanoslit mode of CdS and CdTe CNPs, respectively.

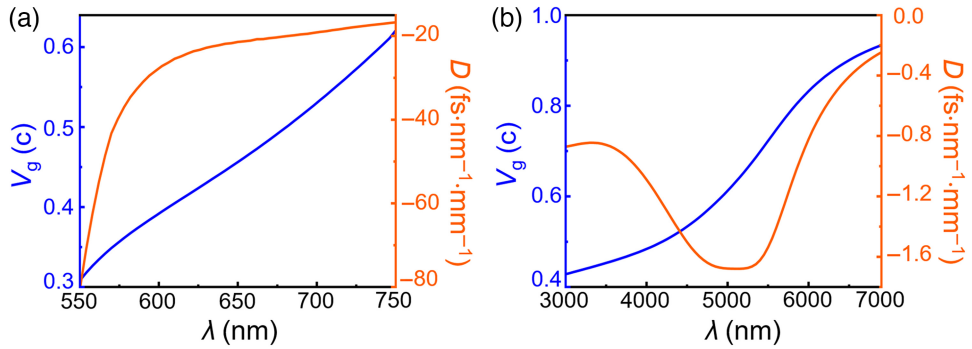

Fig. 6 λ-dependent V_g and D of the nanoslit mode in a CdS CNP at (a) visible spectrum with $d = 140$ nm and (b) MIR spectrum with $d = 1$ μm. In all calculations, w is assumed to be 1 nm and r is assumed to be 5 nm.

In addition, CNPs assembled with CdTe nanowires (with material index n_{CdTe} of ~2.68 versus $n_{\mathrm{CdS}} \sim 2.27$ at 3.7-μm wavelength)[50] have also been investigated [Figs. 5(b) and 5(e)], showing the possibility of obtaining a tighter field confinement and a higher $R_{P1/B}$ by using higher-index materials. For reference, a 0.23-nm (x axis) FWHM of the field intensity [Fig. 5(b), blue solid line] corresponds to $\sim\lambda/20{,}000$ confinement.

6 Dispersion of the Nanoslit Mode

Benefiting from the waveguiding scheme, it is also possible to generate broadband or ultrafast-pulsed sub-nm-confined optical fields in the nanoslit by selecting appropriate input light sources. In such a case, group velocity (V_g) and dispersion (D) should be considered.[51] Figure 6 gives the calculated V_g and D of the TE_0-like nanoslit mode in visible and MIR spectral ranges, respectively. Due to the relatively small nanowire diameter (i.e., $d \cdot n/\lambda < 1$), the increasing λ leads to the increasing fractional power in the air, thus increasing V_g with negative dispersion in both spectral ranges. The larger D in the visible spectrum is due to the larger material dispersion near the bandgap of CdS (~520 nm).

Although the dispersion of the nanoslit mode is orders of magnitude larger than those of conventional waveguides (e.g., ~0.01 fs $\cdot$ nm^{-1} $\cdot$ mm^{-1} at 1550 nm for single-mode fiber[51,52]), the short length of the CNP used for in-coupling and mode evolution (e.g., <10 μm) has little influence on the pulse width. For example, after waveguiding through a 10-μm-length CdS CNP, a 100-fs pulse with a central wavelength of 650 nm and a bandwidth of 30 nm will be broadened ~6 fs in pulse width.

7 Conclusion and Discussion

Based on the numerical calculation, we have demonstrated a waveguiding scheme to generate a sub-nm-confined optical field in a TE_0-like nanoslit mode. We show that waveguiding mode from a standard optical fiber (or on-chip waveguide) can be efficiently coupled into a CNP waveguide and evoluted into a high-purity TE_0-like nanoslit mode within a propagation length less than 10 μm. Using a tapered fiber (or on-chip waveguide) for matching the n_{eff} of the TE_0-like nanoslit mode within a broad spectral range, the waveguiding scheme can work in broadband with a coupling efficiency up to 95% and a bandwidth up to 200 nm. At both visible and MIR bands, within the slit region, the diffraction-limited mode can offer an optical confinement down to ~0.3 nm × 3.3 nm (i.e., $\sim\lambda/2000$ in visible and $\sim\lambda/20{,}000$ in MIR in the tightest-confinement dimension) and a peak-to-background ratio ~30 dB. Benefiting from the short length required for mode coupling and evolution, ultrafast pulses from outer sources can also be converted into a TE_0-like nanoslit mode to offer a sub-nm-confined ultrafast pulsed field with mild dispersion.

Compared with the previous lasing configuration, the waveguiding scheme proposed here is basically a linear optical system, which not only simplifies the complicated lasing system into a linear waveguiding system but also offers great flexibilities for broadband and/or ultrafast pulsed operation, as well as linear combination of multiple sub-nm optical fields with engineerable spatial, spectral, and time sequence in a single output. As the field confinement demonstrated here reaches the same scale of a single small molecule, such a field can offer a spatially inhomogeneous and asymmetric optical field with a large field gradient at the scale of a chemical bond or even an atom, and may thus offer an efficient and flexible platform for exploring light–matter interactions on single molecule or atom level, and developing optical technologies ranging from superresolution nanoscopy,[21] atom/molecule manipulation,[53] to ultrasensitivity detection.[54]

Acknowledgments

The authors thank Professor Y. Ron Shen from the University of California, Berkeley, for helpful discussion. This work was supported by the National Key Research and Development Program of China (2018YFB2200404), the New Cornerstone Science Foundation, the National Natural Science Foundation of China (92150302 and 62175213), the Natural Science Foundation of Zhejiang Province (LR21F050002), and the Fundamental Research Funds for the Central Universities.

References

1. V. R. Almeida et al., "Guiding and confining light in void nanostructure," *Opt. Lett.* **29**(11), 1209–1211 (2004).
2. J. T. Robinson et al., "Ultrasmall mode volumes in dielectric optical microcavities," *Phys. Rev. Lett.* **95**(14), 143901 (2005).
3. C. Caër et al., "Extreme optical confinement in a slotted photonic crystal waveguide," *Appl. Phys. Lett.* **105**(12), 121111 (2014).
4. R. M. Bakker et al., "Magnetic and electric hotspots with silicon nanodimers," *Nano Lett.* **15**(3), 2137–2142 (2015).

5. S. Hu and S. M. Weiss, "Design of photonic crystal cavities for extreme light concentration," *ACS Photonics* **3**(9), 1647–1653 (2016).
6. D. N. Basov et al., "Polaritons in van der Waals materials," *Science* **354**(6309), aag1992 (2016).
7. H. Choi, M. Heuck, and D. Englund, "Self-similar nanocavity design with ultrasmall mode volume for single-photon nonlinearities," *Phys. Rev. Lett.* **118**(22), 223605 (2017).
8. S. Hu et al., "Experimental realization of deep-subwavelength confinement in dielectric optical resonators," *Sci. Adv.* **4**(8), eaat2355 (2018).
9. J. J. Baumberg et al., "Extreme nanophotonics from ultrathin metallic gaps," *Nat. Mater.* **18**(7), 668–678 (2019).
10. M. Albrechtsen et al., "Nanometer-scale photon confinement in topology-optimized dielectric cavities," *Nat. Commun.* **13**(1), 6281 (2022).
11. H. Ling, J. B. Khurgin, and A. R. Davoyan, "Atomic-void van der Waals channel waveguides," *Nano Lett.* **22**(15), 6254–6261 (2022).
12. K. P. Arnold et al., "Photonic crystals with split ring unit cells for subwavelength light confinement," *Opt. Lett.* **47**(3), 661–664 (2022).
13. Q. Quan, I. Bulu, and M. Lončar, "Broadband waveguide QED system on a chip," *Phys. Rev. A* **80**(1), 011810 (2009).
14. F. Benz et al., "Single-molecule optomechanics in 'picocavities,'" *Science* **354**(6313), 726–729 (2016).
15. L. Sortino et al., "Bright single photon emitters with enhanced quantum efficiency in a two-dimensional semiconductor coupled with dielectric nano-antennas," *Nat. Commun.* **12**(1), 6063 (2021).
16. P. G. Zotev et al., "Transition metal dichalcogenide dimer nanoantennas for tailored light-matter interactions," *ACS Nano* **16**(4), 6493–6505 (2022).
17. Y. Meng et al., "Bright single-nanocrystal upconversion at sub 0.5 W cm^{-2} irradiance via coupling to single nanocavity mode," *Nat. Photonics* **17**(1), 73–81 (2022).
18. E. Betzig and J. K. Trautman, "Near-field optics: microscopy, spectroscopy, and surface modification beyond the diffraction limit," *Science* **257**(5067), 189–195 (1992).
19. N. Fang et al., "Sub-diffraction-limited optical imaging with a silver superlens," *Science* **308**(5721), 534–537 (2005).
20. L. Wang and X. F. Xu, "High transmission nanoscale bowtie-shaped aperture probe for near-field optical imaging," *Appl. Phys. Lett.* **90**(26), 261105 (2007).
21. B. Yang et al., "Sub-nanometre resolution in single-molecule photoluminescence imaging," *Nat. Photonics* **14**(11), 693–699 (2020).
22. M. Born, E. Wolf, and A. B. Bhatia, *Principles of Optics*, 7th ed., Cambridge University Press, Cambridge (2019).
23. P. Wang et al., "Molecular plasmonics with metamaterials," *Chem. Rev.* **122**(19), 15031–15081 (2022).
24. W. Li et al., "Bright optical eigenmode of 1 nm^3 mode volume," *Phys. Rev. Lett.* **126**(25), 257401 (2021).
25. J. J. Baumberg, "Picocavities: a primer," *Nano Lett.* **22**(14), 5859–5865 (2022).
26. R. F. Oulton et al., "Plasmon lasers at deep subwavelength scale," *Nature* **461**(7264), 629–632 (2009).
27. R. F. Oulton et al., "A hybrid plasmonic waveguide for subwavelength confinement and long-range propagation," *Nat. Photonics* **2**(8), 496–500 (2008).
28. R. Zhang et al., "Chemical mapping of a single molecule by plasmon-enhanced Raman scattering," *Nature* **498**(7452), 82–86 (2013).
29. M. E. Stewart et al., "Nanostructured plasmonic sensors," *Chem. Rev.* **108**(2), 494–521 (2008).
30. H. Wu et al., "Plasmonic nanolasers: pursuing extreme lasing conditions on nanoscale," *Adv. Opt. Mater.* **7**(17), 1900334 (2019).
31. F. Wang and Y. R. Shen, "General properties of local plasmons in metal nanostructures," *Phys. Rev. Lett.* **97**(20), 206806 (2006).
32. I. Bialynicki-Birula and Z. Bialynicka-Birula, "Uncertainty relation for photons," *Phys. Rev. Lett.* **108**(14), 140401 (2012).
33. I. Bialynicki-Birula and Z. Bialynicka-Birula, "Heisenberg uncertainty relations for photons," *Phys. Rev. A* **86**(2), 022118 (2012).
34. H. Wu et al., "Photonic nanolaser with extreme optical field confinement," *Phys. Rev. Lett.* **129**(1), 013902 (2022).
35. L. M. Tong et al., "Photonic nanowires directly drawn from bulk glasses," *Opt. Express* **14**(1), 82–87 (2006).
36. T. G. Tiecke et al., "Efficient fiber-optical interface for nanophotonic devices," *Optica* **2**(2), 70–75 (2015).
37. R. E. Treharne et al., "Optical design and fabrication of fully sputtered CdTe/CdS solar cells," *J. Phys.: Conf. Ser.* **286**(1), 012038 (2011).
38. R. Yan, D. Gargas, and P. D. Yang, "Nanowire photonics," *Nat. Photonics* **3**(10), 569–576 (2009).
39. L. N. Quan et al., "Nanowires for photonics," *Chem. Rev.* **119**(15), 9153–9169 (2019).
40. X. Guo, Y. B. Ying, and L. M. Tong, "Photonic nanowires: from subwavelength waveguides to optical sensors," *Acc. Chem. Res.* **47**(2), 656–666 (2014).
41. R. J. Black and L. Gagnon, *Optical Waveguide Modes: Polarization, Coupling and Symmetry*, 1st ed., McGraw-Hill Professional Publishing, New York (2010).
42. F. Salvat-Pujol and J. S. Villarrubia, "Conventional vs. model-based measurement of patterned line widths from scanning electron microscopy profiles," *Ultramicroscopy* **206**, 112819 (2019).
43. C. G. Xin et al., "Self-phase modulation in single CdTe nanowires," *Opt. Express* **27**(22), 31800–31809 (2019).
44. D. W. Langer, "Temperature and pressure dependence of the index of refraction of CdS," *J. Appl. Phys.* **37**(9), 3530–3532 (1966).
45. K. J. Savage et al., "Revealing the quantum regime in tunnelling plasmonics," *Nature* **491**(7425), 574–577 (2012).
46. G. Toscano et al., "Resonance shifts and spill-out effects in self-consistent hydrodynamic nanoplasmonics," *Nat. Commun.* **6**(1), 7132 (2015).
47. J. Khurgin et al., "Landau damping and limit to field confinement and enhancement in plasmonic dimers," *ACS Photonics* **4**(11), 2871–2880 (2017).
48. Y. Yang et al., "A general theoretical and experimental framework for nanoscale electromagnetism," *Nature* **576**(7786), 248–252 (2019).
49. D. Minoli, *Nanotechnology Applications to Telecommunications and Networking*, 1st ed., Wiley, Hoboken (2005).
50. E. D. Palik, *Handbook of Optical Constants of Solids II*, 2nd ed., Academic Press, New York (1991).
51. Z. X. Shi et al., "Miniature optical correlator in a single-nanowire Sagnac loop," *ACS Photonics* **7**(11), 3264–3269 (2020).
52. A. Sugimura et al., "Wavelength dispersion characteristics of single-mode fibers in low-loss region," *IEEE J. Quantum Electron.* **16**(2), 215–225 (1980).
53. J. Weiner et al., "Experiments and theory in cold and ultracold collisions," *Rev. Mod. Phys.* **71**(1), 1–85 (1999).
54. L. M. Tong, "Micro/nanofibre optical sensors: challenges and prospects," *Sensors* **18**(3), 903 (2018).
55. G. Y. Zhai and L. M. Tong, "Roughness-induced radiation losses in optical micro or nanofibers," *Opt. Express* **15**(21), 13805–13816 (2007).
56. A. V. Kovalenko, V. N. Kurashov, and A. V. Kisil, "Radiation losses in optical nanofibers with random rough surface," *Opt. Express* **16**(8), 5797–5806 (2008).

Liu Yang is currently a PhD student in the College of Optical Science and Engineering at Zhejiang University. He received his BS degree in optical science and engineering from Nanjing University of Aeronautics and Astronautics in 2019. His current research focuses on nanophotonics.

Zhanke Zhou is currently a PhD student in the College of Optical Science and Engineering at Zhejiang University, China. He received his BS degree in optical science and engineering from Tianjin University in 2021. His current research focuses on nanophotonics.

Hao Wu is currently a joint post-doctor of Hangzhou Hikvision Digital Technology Co., Ltd., Zhejiang, China and the College of Optical Science and Engineering at Zhejiang University, China. He received his PhD in the College of Optical Science and Engineering at Zhejiang University. His current research focuses on lidar technology and algorithm.

Hongliang Dang is currently a PhD student in the College of Optical Science and Engineering at Zhejiang University, China. He received his BS degree in Optical Science and Engineering from Nanjing University of Aeronautics and Astronautics, China in 2022. His current research focuses on nanophotonics.

Yuxin Yang is currently a PhD student in the College of Optical Science and Engineering at Zhejiang University, China. She received her BS degree from Nanjing University of Posts and Telecommunications in 2017. Her current research focuses on nanophotonics.

Jiaxin Gao is currently an undergraduate student in the College of Optical Science and Engineering at Zhejiang University, China. Her current research interest is nanophotonics.

Xin Guo is currently an associate professor in the College of Optical Science and Engineering at Zhejiang University, China. Her main research interests include nanofiber, nanoplasmonics, and nanophotonic devices.

Pan Wang is currently a professor in the College of Optical Science and Engineering at Zhejiang University, China. His main research interests include nanoplasmonics and quantum plasmonics.

Limin Tong is currently a professor in the College of Optical Science and Engineering at Zhejiang University, China. His main research interests include nanophotonics, nanoplasmonics, and fiber optics, with emphases on nanowaveguides and nanophotonic devices. He is an OPTICA fellow.